Turbulent Heat Transfer in A Channel Flow with Arbitrary Directional System Rotation

Haibin Wu* and Nohuhide Kasagi
Department of mechanical engineering, The University of Tokyo,
Hongo 7-3-1, Bunkyo ku, Tokyo, Japan
*Corresponding author: Tel.: +81-3-5841-6418; Fax: +81-3-5800-6999
E-mail address: wu@thtlab.t.u-tokyo.ac.jp (Haibin Wu)

Abstract

Arbitrary directional system rotation of a channel flow can be decomposed into simultaneous componential rotations in the three orthogonal directions. In order to study its effect on turbulent heat transfer, three typical cases, i.e., combined spanwise and streamwise (Case I), streamwise and wall-normal (Case II), and wall-normal and spanwise rotations (Case III), are simulated with two of the three coordinate-axial rotations imposed on the system. In Case I, the effect of spanwise rotation dominates the heat transfer mechanism when the two componential rotation rates are comparable. However, if the streamwise rotation is much stronger than the spanwise rotation, the turbulent heat transfer can be enhanced on the two walls, but more strikingly on the suction side. In Case II, even though no explicit spanwise rotation is imposed on the system, the combined rotations also bring the enhancement/reduction of turbulent heat transfer on the pressure/suction side, respectively, which is similar to that in a spanwise rotating channel flow. In Case III, the spanwise rotation effect is still obvious, however, its effect is reduced somewhat due to the redirection of the mean flow by the wall-normal rotation.

Keywords: *turbulent heat transfer, rotating channel flow, direct numerical simulation, combined system rotations*

Int. J. Heat Mass Transfer 47, 4579-4591 (2004)

Nomenclature

C_f	friction coefficient, $2\tau_w / \rho U_b^2$
MP	Mean gradient production
Nu	Nusselt number, $2q_w\delta/\lambda\lvert T_b - T_w\rvert$
$\tilde{p}$	instantaneous pressure
Pr	Prandtl number
q_w	wall heat flux, $-\lambda(d\Theta/dy)_w$
Re_b	bulk Reynolds number, $2U_b\delta/\nu$
$\mathrm{Re}_{\tau 0}$	Reynolds number, $u_{\tau 0}\delta/\nu$
Ro	absolute rotation number, $(Ro_j Ro_j)^{1/2}$
Ro_j	rotation number in x_j-direction, $2\Omega_j\delta/u_{\tau 0}$
RP	rotation production
U, W	Mean velocities in x- and z-directions
$\underline{U}, \underline{W}$	Mean velocities in x'- and z'-directions
$\tilde{u}_j$	instantaneous velocity in x_j-direction
u, v, w	velocity fluctuations
U_b, W_b	bulk mean velocities in x- and z-directions
u_τ	friction velocity, $\sqrt{\tau_w/\rho}$
$\overline{u_j\theta}$	turbulent heat flux in x_j-direction

Greek symbols

α	Mean flow angle, $\tan^{-1}(W_b/U_b)$
δ	half channel width
λ	thermal conductivity
μ	dynamic viscosity
$\tilde{\theta}$	instantaneous temperature
Θ	mean temperature
θ	temperature fluctuation
ρ	density
τ_w	wall shear stress
Ω_j	angular velocity in x_j-direction

Subscript and superscript

b	bulk mean
p	values on the pressure side
rms	root mean square
s	values on the suction side
w	values on the wall
0	values in a non-rotating channel
+	quantities non-dimensionalized by by τ_w, q_w, ρ and μ.

1. Introduction

In the past several decades, experimental and numerical investigations have been made to explore the rotating turbulent flow mechanics, which plays important roles in many engineering applications. In this type of flows, the Coriolis and centrifugal forces arising from system rotation alter the mean flow patterns as well as the turbulent structures simultaneously, so that the associated turbulent heat transfer is also significantly changed. Making clear the underlying mechanism of heat transfer in rotating flows is a key to further improve the efficiency of rotating machinery.

It is well known that the spanwise rotation (SP) imposed on a channel flow can enhance turbulence on the pressure side, while reduce it on the suction side [1-8]. Coinciding with this tendency, the Nusselt number is also increased on the pressure side and decreased on the suction side [8]. The profile of the mean temperature in the core region becomes more uniform and its value is closer to the pressure wall temperature as increasing the rotation rate. On the suction side, however, the increase of the rotation rate makes the distribution of the mean temperature similar to that in a laminar flow. The root-mean-square (rms) temperature fluctuation as well as the turbulent heat fluxes of $\overline{u\theta}$ and $\overline{v\theta}$ become much weaker at higher rotation rates [8].

In a streamwise rotating channel, the profile of the mean temperature is still skew-symmetric with respect to the channel center, but a more flattened profile appears in the core region at high rotation rates [7-9]. The streamwise rotation (ST) enhances the Nusselt number on both walls and induces a new turbulent heat flux term of $\overline{w\theta}$, whose absolute value increases obviously with the rotation rate [8].

The wall-normal rotation (WN) induces a strong spanwise mean velocity in a channel flow, so that the absolute mean flow tilts to the spanwise direction [7,8]. This redirection of the mean flow greatly enhances the turbulent heat flux term of $\overline{w\theta}$, whose distribution becomes similar to $\overline{u\theta}$. The influence of WN on $\overline{v\theta}$ is quite small, so that the profile of this term keeps nearly unchanged.

These studies provide basic knowledge on the heat transfer in three typical cases of rotating channel flows (defined as orthogonal modes), in which the rotating axis is parallel to one of the orthogonal (streamwise, wall-normal and spanwise) directions. In real applications, however, the rotating vector direction can be arbitrary. Although such an arbitrary rotation can be decomposed into simultaneous componential rotations in the directions of the coordinate axes, its effect cannot be determined directly from the latter due to the nonlinear nature of turbulence. Therefore, it is necessary to further consider the effect of arbitrary rotation on turbulent heat transfer. In the present study, we design three ideal cases by combining two of the three orthogonal rotations, that is, combined SP/ST, ST/WN and WN/SP, to instigate the effect of combined orthogonal rotations on turbulent heat transfer.

2. Numerical formulation

We consider a turbulent flow between two parallel infinite walls, which is driven by a mean pressure gradient $-dP/dx$ in the *x*-direction. The computation domain and coordinate system for this flow are schematically shown in Fig.1. The mean pressure gradient in the *x*-direction is adjusted at each computation time step to keep a constant bulk mean velocity in this direction and the corresponding bulk Reynolds number Re_b is equal to 4560. No-slip boundary conditions are used for velocities on the walls.

The temperatures on the two walls are assumed to be constant with a higher one on the lower wall, but the buoyancy arising from the temperature difference is neglected, since the objective of the present study is to explore the effect of system rotation. Therefore, the heat transfer can be regarded as transport of a passive scalar, which has no active effects on the flow field. Fully developed states are presumed for both the flow and thermal fields, and thus periodic boundary conditions are used in the *x*- and *z*-directions.

This problem can be described by a set of hydrodynamic equations for an incompressible flow

in a rotating reference frame as follows:

$$\frac{\partial \tilde{u}_i}{\partial t} = -\frac{\partial \tilde{p}}{\partial x_i} + \frac{1}{\mathrm{Re}_{\tau 0}} \frac{\partial^2 \tilde{u}_i}{\partial x_j^2} - \tilde{u}_j \frac{\partial \tilde{u}_i}{\partial x_j} - \varepsilon_{ijk} Ro_j \tilde{u}_k , \tag{1}$$

$$\frac{\partial \tilde{u}_i}{\partial x_i} = 0 , \tag{2}$$

$$\frac{\partial \tilde{\theta}}{\partial t} = \frac{1}{\mathrm{Re}_{\tau 0} \mathrm{Pr}} \frac{\partial^2 \tilde{\theta}}{\partial x_j \partial x_j} - \tilde{u}_j \frac{\partial \tilde{\theta}}{\partial x_j} , \tag{3}$$

where Ro_j is the componential rotation number in the x_j-direction. These equations are non-dimensionalized by the channel half width δ, the friction velocity $u_{\tau 0}$ in a non-rotating channel and the temperature difference ΔT between the two walls. The fluid is assumed to be air, so the Prandtl number Pr is equal to 0.71.

Following Kim et al. [10], Eqs. (1) and (2) can be reduced to yield a fourth-order equation for $\tilde{v}$, and a second-order equation for the normal component of vorticity. A spectral method is used for the spatial discretization with Fourier series expansions applied in the *x*- and *z*-directions and Chebyshev polynomial expansion in the *y*-direction. A mesh system of $128 \times 97 \times 128$ grids is employed in the *x*-, *y*- and *z*-directions, respectively, and the 3/2 rule is used to remove the aliasing errors. In the time advancement, the Crank-Nicolson scheme is applied for the viscous terms and the second-order Adam-Bashforth scheme for the nonlinear and Coriolis force terms, respectively. The Courant number is less than 0.3 to ensure the numerical stability. After both the flow and thermal fields reach fully developed states, the time integration is further extended over a time length of $12\delta / u_{\tau 0}$ for sampling the statistics.

3. Results and discussions

In the present study, three cases are simulated as summarized in Table 1. In Case I, the spanwise rotation number is kept constant ($Ro_z = 2.5$) with the streamwise rotation number Ro_x increased

to 15. In Cases II and III, the wall-normal rotation number is kept constant ($Ro_y = 0.04$) with Ro_x and Ro_z increased to 15.

3.1 Case I (SP/ST)

At low Ro_x, the mean temperature has a nearly linear distribution in the core region, and its value is much closer to the pressure wall temperature as shown in Fig. 2(a). These properties are the same as those in a spanwise rotating channel, which reveals the dominant effect of SP. As Ro_x increases, the mean temperature in the core region gradually decreases, and the linear distribution disappears at high Ro_x. The mean temperature in wall units is shown in Fig. 2(b). The profile of the mean temperature on the suction side moves away from the linear relation of $\Theta^+ = \mathrm{Pr}\cdot y^+$ and approaches to the profile on the pressure side with Ro_x increased. This trend suggests the enhancement of turbulent heat transfer on the suction side by ST. On the pressure side, however, the profile of the mean temperature is almost constant, which indicates that the local heat transfer mechanism does not change.

The Nusselt number in Case I, normalized by the corresponding value in a non-rotating channel, is depicted in Fig. 3. It shows that Nu increases obviously with Ro_x on both walls. This tendency is different from that of the friction coefficient, which increases on the suction side, but nearly constant on the pressure side [11].

In the present study, the wall temperatures are kept constant and no inner heat sources are imposed, so that the following equation holds for the fully developed thermal filed,

$$0 = \frac{1}{\mathrm{Re}_{\tau 0}\,\mathrm{Pr}}\frac{d^2\Theta}{dy^2} - \frac{d\overline{v\theta}}{dy}. \tag{4}$$

Integrating this equation from the lower to upper walls yields

$$\left.\frac{d\Theta}{dy}\right|_{y=1} = \left.\frac{d\Theta}{dy}\right|_{y=-1}. \tag{5}$$

Equation (5) reveals that the heat fluxes on the two walls should be the same in a fully developed thermal field. When ST enhances the wall heat flux on the suction side, the counterpart on the pressure side should be increased by the same amount. According to the definition of Nu, its change also depends on the difference between the bulk-mean and wall temperatures. As Ro_x increases, the difference between Θ_b and Θ_p increases, while that between Θ_b and Θ_s decreases as shown in Fig. 2(a), so that Nu on the suction side increases more than on the pressure side.

The increase of the streamwise rotation rate makes the rms temperature fluctuation enhanced gradually on both walls, but more remarkably on the pressure side, as shown in Fig. 4(a). The budgets of the temperature variance $\overline{\theta^2}$ are shown in Figs. 4(b) and (c), in which the molecular diffusions are omitted for brevity. On the pressure side, although strong ST is imposed to the system, the relative magnitudes and the distributions of all terms in the budget of $\overline{\theta^2}$ are almost invariant. This consistency reveals that the mechanism to produce $\overline{\theta^2}$ is unchanged, and the enhancement of θ_{rms} is mainly due to the increase of the temperature gradient. On the suction side, however, the peaks of the mean production and the dissipation rate become much closer to the wall when Ro_x is increased to 15, so that the peak of θ_{rms} also appears closer to the wall as shown in Fig. 4(a).

The growth of the temperature gradient on both sides increases the mean production term $MP_{u\theta}$ as shown in Table 2. Furthermore, the mean velocity gradient and the Reynolds stress term $\overline{uv}$ are obviously enhanced on the suction side, while kept nearly constant on the pressure side [11], resulting in much larger enhancement of $MP_{u\theta}$ on the suction side. In accordance with this change, the heat flux term $\overline{u\theta}$ is increased more strikingly on the suction side as shown in Fig. 5(a). The

increase of Ro_x induces the enhancement of the rotational production $RP_{v\theta}$ in Table 2, and the mean production $MP_{v\theta}$ also increases with the temperature gradient, so that the heat flux term $\overline{v\theta}$ is enhanced in the whole channel [see Fig.5(b)].

Due to ST, a new turbulent heat flux term $\overline{w\theta}$ comes forth, and increases with Ro_x on both walls, but more obviously on the suction side as shown in Fig. 5(c). In the budgets of $\overline{w\theta}$ as shown in Figs. 6(a) and (b), the correlation between pressure and temperature gradient $\overline{p\partial\theta/\partial z}$ serves as the dominant source term and is mainly balanced by the rotational production in the whole channel except in the near-wall region. In the buffer layer, the mean production, the dissipation rate and the turbulent and molecular diffusions play more significant roles, but their values are still smaller than the formers.

The instantaneous velocity vectors and temperature in a *y*-*z* cross section of a spanwise rotating channel flow with $Ro_z = 2.5$ are shown in Fig. 7(a). Although strongly blurred by the local vortices, two pairs of counter-rotating roll cells can be detected from the velocity field. These roll cells convect fluids of different temperatures from the pressure and suction sides to the core region, and well mix them through the rotational motion. Consequently, the mean temperature in the core region tends to be uniform in a spanwise rotating channel flow. The roll cells are much closer to the pressure side, so that more fluids with higher temperature can be convected to the core region. As a result, the mean temperature in the core region becomes closer to the pressure wall temperature.

The streamlines of roll cells and the contours of temperature fluctuations averaged in the *x*-direction and over a time period of $4\delta/u_{\tau 0}$ are shown in Fig. 7(b). The temperature fluctuations from the local vortical motions are greatly diminished in the average and only those from the persistent large-scale roll cells can survive. In Fig. 7(b), it is clear that when the roll cells transport high-temperature fluids from the core region to the suction side or low-temperature fluids in the reverse direction, large temperature fluctuations can be produced on the suction side, since the

temperature difference is comparatively large. This effect brings positive turbulent diffusion in the near-wall region, while negative in the core region, in the budget of $\overline{\theta^2}$ as shown in Fig. 4(c). On the pressure side, however, much weaker temperature fluctuations are generated through the convection, because the temperature difference there is much smaller than on the suction side. The instantaneous temperature fluctuations in Fig. 7(a) show a similar trend that the strong temperature fluctuations centralize on the suction side.

If strong ST is imposed to the system, the regular distribution of the large-scale roll cells from SP is greatly influenced as shown in Fig. 8(a). Although two large-scale cells rotating in the positive streamwise (clockwise) direction still exist in the channel, the negative streamwise (counter-clockwise) rotating ones are strongly blurred by ST [11]. Some new vortices whose diameter is smaller than the roll cells appear in the channel, especially on the suction side. Most of these vortices rotate in the positive streamwise direction [11]. These vortices convect more fluids of low temperature from the suction side to the core region, and consequently the mean temperature in the core region decreases as shown in Fig. 2(a). This reduction reduces the temperature difference on the suction side, while increases it on the pressure side. When the local or large-scale vortices convect fluids locally or between the near-wall and core regions on the pressure side, much stronger temperature fluctuations can be generated due to the increase of the temperature difference. On the suction side, the convection becomes much stronger due to the appearance of new vortices, but the temperature difference becomes smaller, and therefore the temperature fluctuations are only enhanced slightly as shown in Fig. 4(a).

The streamwise rotation enhances the vortices rotating in the same direction, including the large-scale and near-wall vortices, whereas diminishes others rotating oppositely [8, 11]. In the present case, the positive streamwise-rotating vortices prevail over the negative rotating ones. Since the lower wall is heated, the positive rotating vortices produce positive-temperature fluctuations on the left and negative on the right as shown in Fig. 8(b). As a result, the temperature gradient term

$\partial\theta/\partial z$ becomes negative inside the vortices. Furthermore, the pressures inside the vortices are very low due to the rotation, and hence the multiplication of these two terms becomes positive. This explains why the correlation between the pressure and the temperature gradient $\overline{p\,\partial\theta/\partial y}$ balances with the negative rotation production in the budget of $\overline{w\theta}$ as depicted in Fig. 6.

3.2 Case II (ST/WN)

The wall-normal rotation induces a strong spanwise mean velocity, which makes the absolute mean flow tilt to the spanwise direction. If a rotation in the x-direction is further imposed, this rotation can be approximately decomposed into two componential rotations in the absolute mean flow direction and perpendicular to the absolute mean flow [11]. The rotation numbers in these two directions are $Ro_x\cos\alpha$ and $-Ro_x\sin\alpha$, respectively, where α is the tilting angle of the absolute mean flow from the x-direction and defined as $\alpha=\tan^{-1}(W_b/U_b)$. Due to the rotation perpendicular to the absolute mean flow, some effects similar to those of SP arise in the flow field, i.e., the enhancement and reduction of turbulence on the two walls [11]. According to the Coriolis force Ro_xW in the y-direction, the upper wall is defined as the pressure side, while the lower wall as the suction side. This situation is just contrary to that in Case I.

The mean temperature in Case II is shown in Fig. 9(a), from which we can see that the mean temperature in the core region becomes more uniform and its value approaches to the pressure wall temperature. The profile of the mean temperature in wall units on the suction side moves toward the linear relation of $\Theta^+=\mathrm{Pr}\cdot y^+$ with increasing Ro_x, indicating the reduction of the turbulent heat transfer on this side, while the profile on the pressure side keeps a similar distribution, but the slope gradually decreases, as shown in Fig. 9(b).

In general, as Ro_x increases, the relaminarization on the suction side proceeds. However, the profile at $Ro_x=7.5$ returns somewhat from the linear relation on the suction side, revealing that

the enhancement of turbulent activities restarts at this rotation number. This exceptional change is because of the enhancement of the componential rotation in the absolute mean flow direction, which tends to enhance turbulence on the suction side as we discussed in Case I. The effect of this rotation can be also detected from the Nusselt number in Fig. 10, which is in good agreement with the corresponding value in a spanwise rotating channel at low Ro_x, but becomes larger than the latter on the suction side for high rotation numbers.

The rms temperature fluctuation in Case II is shown in Fig. 11(a). Since the two componential rotations act on the thermal field simultaneously, the change of θ_{rms} is not monotonic as that in a spanwise rotating channel flow with increasing Ro_z. However, some similar properties can be found, e.g., the higher rms temperature fluctuation on the suction side. The budgets of the temperature variance $\overline{\theta^2}$ in Figs. 11(b) and (c) resemble those in a spanwise rotating channel as shown in Figs. 4(b) and (c). On the suction side, the peaks of all the terms are much farther from the wall than on the pressure side, and this makes the crest of θ_{rms} move toward the channel center [see Fig. 11(a)].

All the three components of the turbulent heat flux vector in Case II are non-zero as shown in Fig. 12. The combined rotations determines a distribution of $\overline{w\theta}$ quite similar to that of $\overline{u\theta}$, which is negative on the lower-wall side whereas positive on the upper-wall side. The rotational production term $RP_{v\theta}$ in Case II is the multiplication of $\overline{w\theta}$ and Ro_x as shown in Table 2, so that $RP_{v\theta}$ has the same sign as $\overline{w\theta}$ on the two walls. However, the turbulent heat flux term $\overline{v\theta}$ is positive in the whole channel, and thus $RP_{v\theta}$ tends to reduce $\overline{v\theta}$ on the lower-wall side, whereas enhance it on opposite side. With this process, the relaminarization on the lower wall happens. The changes of these turbulent heat flux terms are not monotonic w ith increasing Ro_x due to the combined effects of two componential rotations. The exceptional enhancement of all the

turbulent heat fluxes at $Ro_x = 7.5$ on the suction side coincides with the change of the mean temperature profile and the Nusselt number on the same side.

The turbulent heat flux term $\overline{w\theta}$ plays a very important role in relaminarization on the suction side, so that it is interesting to further explore its budgets as shown in Fig. 13. On the pressure side (upper wall in Case II), the mean production is the dominant source term in the buffer layer, and balances with the dissipation rate, rotational production, and molecular and turbulent diffusions. Farther away from the wall, the correlation between the pressure and temperature gradient and the rotational production become the dominant terms. The mean production remains large in the core region, but its role is minor compared to the former two terms. On the suction side, the mean and rotational productions are negative, giving the negative value of $\overline{w\theta}$ on this side. These two terms are almost in balance with $\overline{p\partial\theta/\partial y}$ except in the neighborhood of the wall.

The instantaneous velocity and temperature fluctuations in Case II are shown in Fig. 14, from which two counter-rotating large-scale vortices can be found. However, the positive rotating vortex of A is obviously stronger and larger than the negative rotating one of B [11]. The vortex of A transports low-temperature fluids effectively from the upper to lower walls and produces very strong temperature fluctuations on the lower-wall side. Meanwhile, the convection by the vortex of B is much weaker compared with that of A. The convection effect of A is similar to that of the roll cells in a spanwise rotating channel flow, which brings an asymmetric distribution of the rms temperature fluctuation, i.e., larger on the suction side (upper-wall side in Case I and lower-wall side in Case II) and smaller on the pressure side. This similarity can be also detected in the budget of $\overline{\theta^2}$ on the suction side, where the turbulent diffusion is positive in the near-wall region but negative in the core region as shown in Fig. 11(c). The scale and strength of A over those of B induce a positive correlation term between the pressure and the temperature gradient $\overline{p\partial\theta/\partial z}$ through the mechanism discussed in Fig. 8(b), so that this correlation becomes a dominant term in

the core region as shown in Figs. 13(a) and (b).

3.2 Case III (WN/SP)

In this case, we investigate whether the effect of SP can be changed with a strong spanwise mean velocity arising from WN. The dominant Coriolis force term $Ro_z U$ in the *y*-direction points to the lower wall, which is defined as the pressure side, while the opposite side is defined as suction side.

The mean temperature in Case III is represented in Fig. 15(a). As Ro_z increases, the mean temperature in the core region approaches to the pressure wall temperature, and its profile becomes almost linear. The temperature gradients on the two walls decrease with increasing Ro_z. The mean temperature in wall units is shown in Fig. 15(b), in which the profile on the suction side moves toward the linear relation of $\Theta^+ = \Pr \cdot y^+$, whereas on the pressure side the slope of the profile decreases slowly. These properties resemble those in a spanwise rotating channel flow. However, due to WN, the relaminarized region on the suction side becomes much narrower and the temperature gradient on the two walls increases obviously, as shown in Fig. 15(c).

Similar to Case II, the spanwise rotation in Case III can be decomposed into two componential rotations in the absolute mean flow direction and perpendicular to the absolute mean flow. The rotation numbers in these two directions are $Ro_z \cos\alpha$ and $Ro_z \sin\alpha$, respectively, where α is again the tilting angle of the absolute mean flow from the *x*-direction. If the Nusselt number is shown as a function of the rotation number $Ro_z \sin\alpha$, it is in good agreement with the corresponding result in a spanwise rotating channel as seen in Fig. 16. This result reflects that the effective “spanwise” rotation number reduces to $Ro_z \sin\alpha$. Here, the “spanwise” refers to the direction perpendicular to the absolute mean flow and parallel to the wall.

The rms temperature fluctuation and two turbulent heat flux terms are shown in Fig. 17. These

quantities possess similar characteristics to those in a spanwise rotating channel flow. The rms temperature fluctuation has larger values on the suction side and gradually decreases on both sides with increasing Ro_z. The peak of this term on the suction side moves towards the channel central part, coinciding with the broadening of the laminar region. The distributions of $\overline{u\theta}$ and $\overline{w\theta}$ are similar and their values decrease on both walls with increasing Ro_z. On the suction side, the peaks of these two terms also gradually leave away from the wall, in accordance with the movement of θ_{rms}.

In a plane channel flow, the temperature fields are highly correlated to the streamwise velocity [12]. It is interesting to further check this relation in the present case, where rotations significantly change the mean flow direction and turbulent structures. The velocity fluctuations in the absolute mean flow direction are calculated as follows,

$$u_a = u\cos\alpha + w\sin\alpha . \tag{6}$$

The streaky structures of the absolute velocity and temperature are shown in Figs. 18(a) and (b), respectively. All the streaky structures tilt to the positive spanwise direction, coinciding with the redirection of the mean flow. The similarity between the streaky structures of velocity and temperature reveals that the temperature in the near-wall region is still highly correlated with the velocity in the absolute mean flow direction. Since we show the structures near the heated wall (pressure wall in Case III), the high-temperature regions are associated with low-velocity fluid and vice versa. The correlation coefficient between the temperature and the absolute velocity in the near-wall region is about 0.8, which is smaller than that in the plane channel without rotation reported by Kim and Moin [12].

The flow field is so sensitive to WN that a strong spanwise mean velocity is produced by a very weak wall-normal rotation rate. If the wall-normal rotation rate is further enhanced, the spanwise mean velocity will be continuously increased, so that the tilting angle of the absolute mean flow to

the spanwise direction will become increasingly larger. Correspondingly, the effect of SP will continue to decrease.

4. Conclusions

The effects of arbitrary directional rotation on turbulent heat transfer are explored through a series of DNS. Three cases, i.e., SP/ST, ST/WN and WN/SP, are considered by combining two of the three orthogonal rotations. When SP and ST exist simultaneously and the rotation rates are comparable, the effect of SP still dominates the heat transfer mechanism across the whole channel, while ST brings some minor changes on the suction side. If ST is much stronger than SP, it enhances the turbulent heat transfer on both walls, but more obviously on the suction side.

In the case of ST/WN, the absolute mean flow is tilted by WN to the spanwise direction, so that the streamwise rotation can be decomposed into two componential rotations in the absolute mean flow direction and perpendicular to that direction. The latter rotation resembles SP and also brings the reduction/enhancement of turbulent heat transfer on the suction/pressure wall, so that the thermal field is like that in a spanwise rotating channel flow.

The effects of SP on the thermal filed are still apparent in the case of WN/SP with a comparatively weak wall-normal rotation. However, the redirection of the mean flow by WN reduces the effective rotation rate perpendicular to the mean flow direction. Therefore, the effects of SP on the thermal field are reduced to some extent compared to those with the same spanwise rotation rates, but no wall-normal rotation.

The present work extends the study of heat transfer in rotating channel flows from orthogonal mode to arbitrary directional rotation. However, the effects of some important parameters, such as the Reynolds and Prandtl numbers, and of the different boundary conditions, have not been touched. These problems will be explored in the future studies.

Acknowledgements

This work was supported through the research project on “Mirco Gas Turbine/Fuel Cell Hybrid-type Distributed Energy System” by the Department of Core Research for Evolutional Science and Technology (CREST) of Japan Science and Technology Corporation (JST).

References

[1] J. P. Johnston, R. M. Halleen, D. K. Lezius, Effects of spanwise rotation on the structure of two-dimensional fully developed turbulent channel flow, Journal of Fluid Mechanics 56 (1972), 533-557.

[2] J. Kim, The effect of rotation on turbulence structure, Proceedings of the Fourth International Symposium on Turbulent Shear Flows, Karlsruhe, Germany, 1982, pp. 6.14-6.19.

[3] U. Piomelli, J. Liu, Large-eddy simulation of rotating channel flows using a localized dynamic model, Physics of Fluids 7 (1995), 839-848.

[4] M. Tsubokura, T. Kobayashi, N. Taniguchi, T. Kogaki, Subgrid scale modeling for turbulence in rotating reference frames, Journal of Wind Engineering and Industrial Aerodynamics 81 (1999), 361-375.

[5] B. E. Launder, D. P. Tselspidakis, B. A. Younis, A second-moment closure study of rotating channel flow, Journal of Fluid Mechanics 183 (1987), 63-75.

[6] R. Kristoffersen, H. I. Andersson, Direct simulations of low-Reynolds-number turbulent flow in a rotating channel, Journal of Fluid Mechanics 256 (1993), 163-197.

[7] O. Elsamni, N. Kasagi, The effects of system rotation with three orthogonal rotating axes on turbulent channel flow, Proceedings of 7th International Congress on Fluid Dynamics and Propulsion, Cairo, Egypt, December18-20, 2001, CD-ROM.

[8] O. Elsamni, Heat and momentum transfer in turbulent rotating channel flow, PhD thesis, University of Tokyo, Tokyo, Japan, 2001.

[9] M. Oberlack, W. Cabot, M. M. Rogers, Turbulent channel flow with streamwise rotation; Lie group analysis, DNS and modeling, Proceedings of the First International Symposium on Turbulence and Shear Flow Phenomena, Santa Barbara, USA, September 12-15, 1999, pp. 85-90.

[10] J. Kim, P. Moin, R. Moser, Turbulence statistics in fully developed channel flow at low Reynolds number, Journal of Fluid Mechanics 177 (1987), 133-166.

[11] H. Wu, N. Kasagi, Effects of combined orthogonal rotations on turbulent channel flow, Physics of Fluids 16 (2004), 979-990.

[12] J. Kim, P. Moin, Transport of passive scalars in a turbulent channel flow, Turbulent Shear Flows 6, (Edited by André, J. C. et al.), 85-96, Springer.

Tables

Table 1 Test Conditions

	Case	Condition I	Condition II
SP/ST	I	$Ro_x = 2.5 \sim 15$	$Ro_z = 2.5$
ST/WN	II	$Ro_x = 2.5 \sim 15$	$Ro_y = 0.04$
WN/SP	III	$Ro_z = 2.5 \sim 15$	$Ro_y = 0.04$

Table 2 Productions due to the mean gradient ($MP_{u_j\theta}$) and rotation ($RP_{u_j\theta}$).

		$\overline{u\theta}$	$\overline{v\theta}$	$\overline{w\theta}$
$MP_{u_j\theta}$		$-\overline{uv}\frac{d\Theta}{dy} - \overline{v\theta}\frac{dU}{dy}$	$-\overline{vv}\frac{d\Theta}{dy}$	$-\overline{vw}\frac{d\Theta}{dy} - \overline{v\theta}\frac{dW}{dy}$
$RP_{u_j\theta}$	Case I	$Ro_z\overline{v\theta}$	$Ro_x\overline{w\theta} - Ro_z\overline{u\theta}$	$-Ro_x\overline{v\theta}$
	Case II	$-Ro_y\overline{w\theta}$	$Ro_x\overline{w\theta}$	$Ro_y\overline{u\theta} - Ro_x\overline{v\theta}$
	Case III	$Ro_z\overline{v\theta} - Ro_y\overline{w\theta}$	$-Ro_z\overline{u\theta}$	$Ro_y\overline{u\theta}$

Figure captions

Fig.1 Computation domain and coordinate system

Fig.2 Mean temperature in Case I. (a) In global coordinate (pressure side: $y=-1$; suction side: $y=1$); and (b) in wall units.

Fig.3 Nusselt number in Case I normalized by the value in a non-rotating channel.

Fig.4 Rms temperature fluctuation and budget of temperature variance $\overline{\theta^2}$ in Case I. (a) Rms temperature fluctuation (pressure side: $y=-1$; suction side: $y=1$); and budgets of $\overline{\theta^2}$ on the pressure side (b) and on the suction side (c) (lines: $Ro_z=2.5$; lines with circles: $Ro_x=15$ and $Ro_z=2.5$; the molecular diffusion term is omitted).

Fig.5 Turbulent heat fluxes in Case I (pressure side: $y=-1$; suction side: $y=1$). (a) $\overline{u\theta}$; (b) $\overline{v\theta}$; and (c) $\overline{w\theta}$.

Fig.6 Budget of $\overline{w\theta}$ at $Ro_x=15$ and $Ro_z=2.5$ in Case I. (a) On the pressure side; and (b) on the suction side.

Fig.7 (a) Instantaneous velocity vectors and temperature fluctuations (black to white: $-0.2<\theta<0.2$) at $Ro_z=2.5$; and (b) streamlines and contours of temperature fluctuations averaged in the *x*-direction and over a time length of $4\delta/u_{\tau 0}$.

Fig.8 (a) Instantaneous velocity and temperature fluctuations (black to white: $-0.2<\theta<0.2$) at $Ro_x=15$ and $Ro_z=2.5$ in Case I; and (b) heat fluxes and low pressure generated by positive streamwise-rotating vortices.

Fig.9 Mean temperature in Case II. (a) In global coordinate (pressure side: $y=1$; suction side: $y=-1$); and (b) in wall units.

Fig.10 Nusselt number in Case II normalized by the value in a non-rotating channel.

Fig.11 Rms temperature fluctuation and budgets of temperature variance $\overline{\theta^2}$ in Case II. (a) Rms

temperature fluctuation (pressure side: $y=1$; suction side: $y=-1$); and budgets of $\overline{\theta^2}$ on the pressure side (b) and on the suction side (c) at $Ro_x=15$ and $Ro_y=0.04$.

Fig.12 Turbulent heat fluxes in Case II (pressure side: $y=1$; suction side: $y=-1$). (a) $\overline{u\theta}$; (b) $\overline{v\theta}$; and (c) $\overline{w\theta}$.

Fig.13 Budgets of $\overline{w\theta}$ at $Ro_x=15$ and $Ro_y=0.04$ in Case II. (a) On the pressure side; and (b) on the suction side.

Fig.14 Instantaneous velocity and temperature fluctuations (black to white: $-0.2<\theta<0.2$) at $Ro_x=15$ and $Ro_y=0.04$ in Case II.

Fig.15 Mean temperature in Case III. (a) In global coordinate (pressure side: $y=-1$; suction side: $y=1$); (b) in wall units; and (c) alteration of the mean temperature by WN.

Fig.16 Nusselt number in Case III normalized by the value in a non-rotating channel.

Fig.17 Turbulent heat fluxes in Case III (pressure side: $y=-1$; suction side: $y=1$). (a) $\overline{u\theta}$; (b) $\overline{v\theta}$; and (c) $\overline{w\theta}$.

Fig. 18 Momentum and thermal streaky structures at $y^+=12$ on the pressure side with $Ro_y=0.04$ and $Ro_z=15$. (a) Velocity fluctuation in the absolute mean flow direction; and (b) temperature fluctuation.

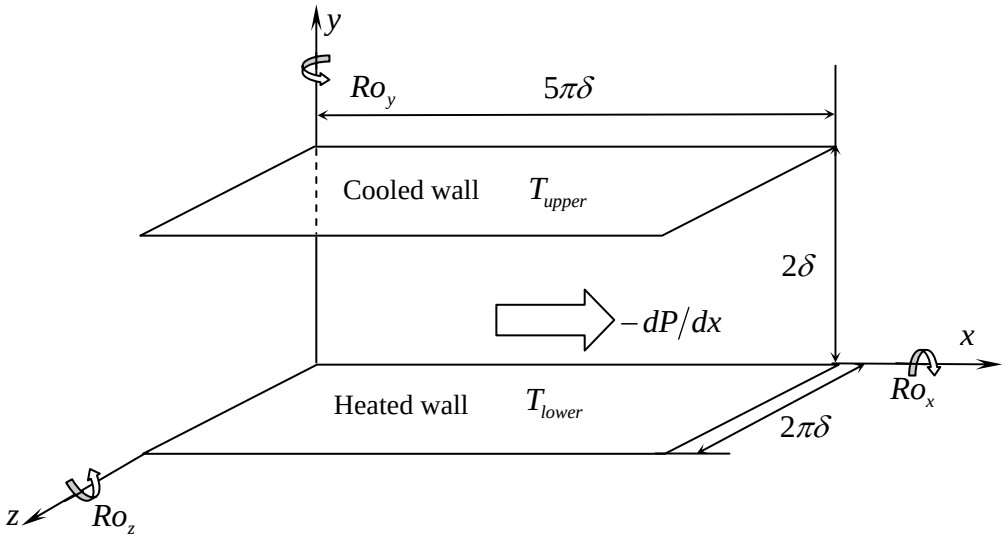
y
Ro_y
5πδ
Cooled wall
T_upper
2δ
−dP/dx
x
Ro_x
Heated wall
T_lower
2πδ
z
Ro_z

Fig. 1

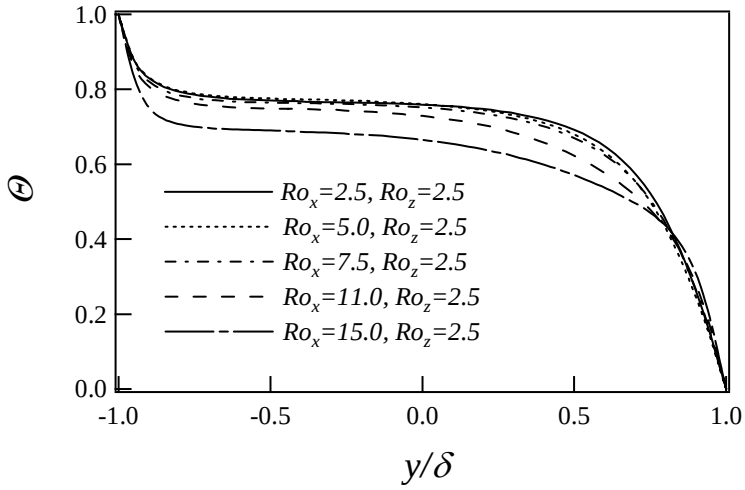
1.0
0.8
0.6
0.4
0.2
0.0
-1.0
-0.5
0.0
0.5
1.0
Θ
Ro_x=2.5, Ro_z=2.5
Ro_x=5.0, Ro_z=2.5
Ro_x=7.5, Ro_z=2.5
Ro_x=11.0, Ro_z=2.5
Ro_x=15.0, Ro_z=2.5
y/δ

(a)

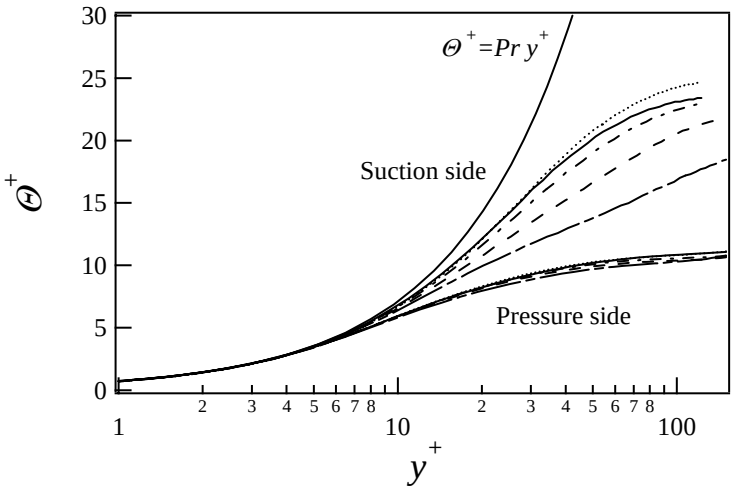
30
25
20
15
10
5
0
1
2
3
4
5
6
7
8
10
100
Θ+=Pr y+
Suction side
Pressure side
Θ+
y+

(b)

Fig. 2

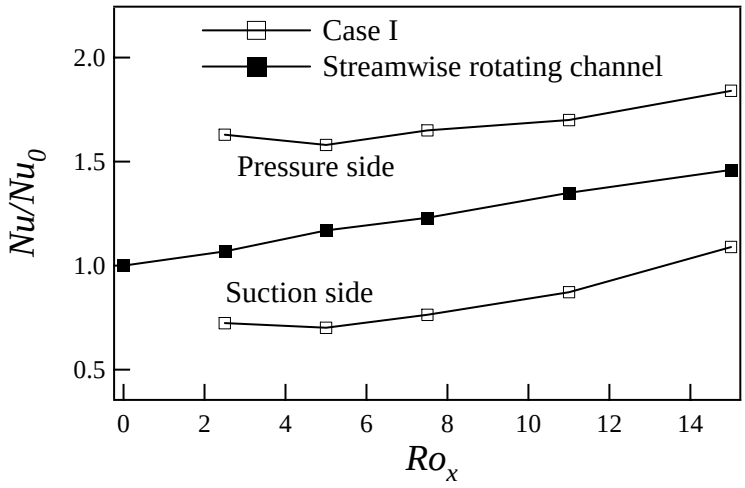
Case I
Streamwise rotating channel
Pressure side
Suction side
Nu/Nu0
Rox
2.0
1.5
1.0
0.5
0
2
4
6
8
10
12
14

Fig. 3

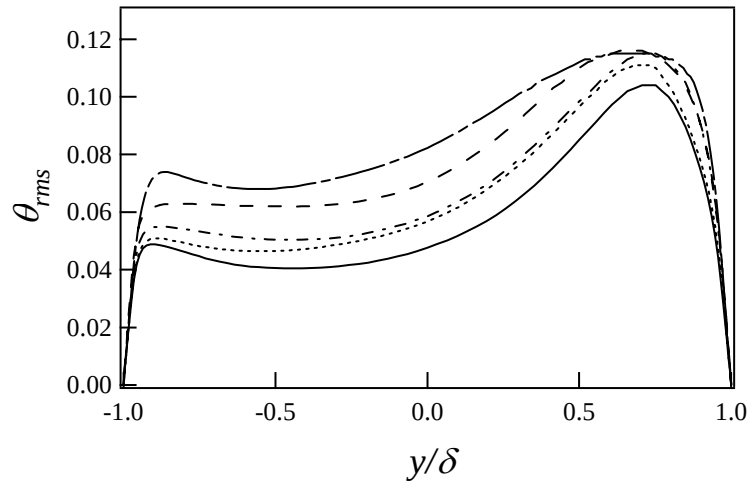
0.12
0.10
0.08
0.06
0.04
0.02
0.00
θ_{rms}
-1.0
-0.5
0.0
0.5
1.0
y/δ

(a)

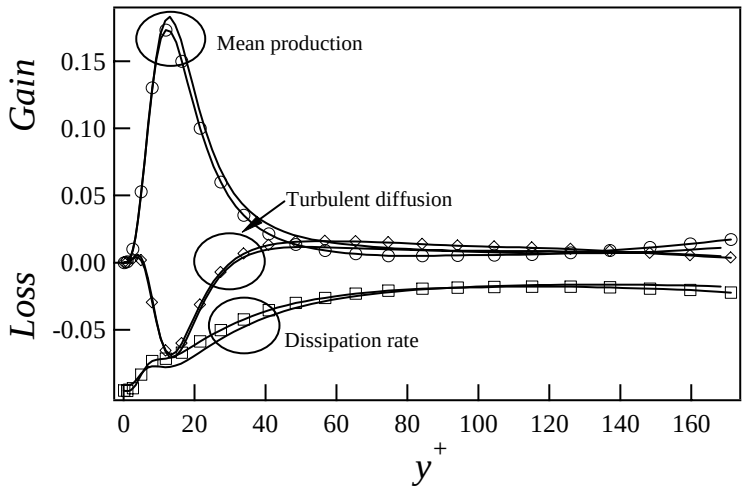
Gain
Loss
Mean production
Turbulent diffusion
Dissipation rate
0.15
0.10
0.05
0.00
-0.05
0
20
40
60
80
100
120
140
160
y^+

(b)

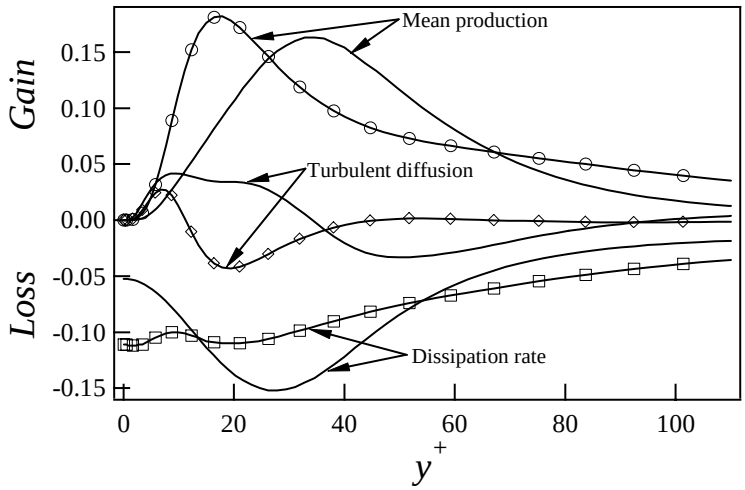
Gain
Loss
Mean production
Turbulent diffusion
Dissipation rate
0.15
0.10
0.05
0.00
-0.05
-0.10
-0.15
0
20
40
60
80
100
y^+

(c)

Fig. 4

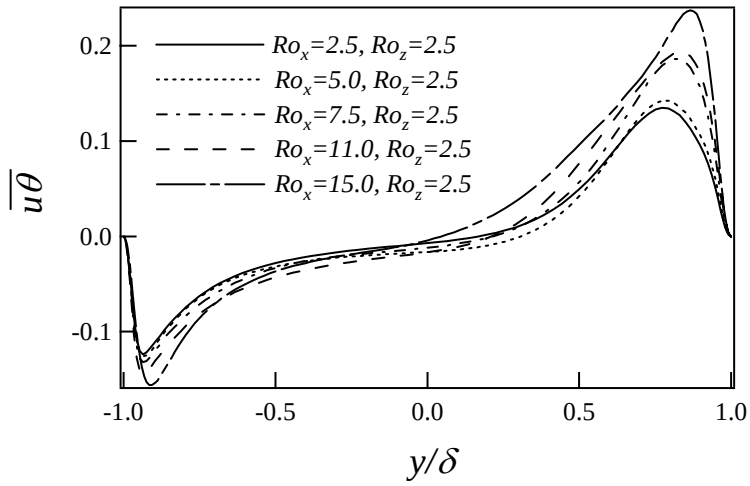
Ro_x=2.5, Ro_z=2.5
Ro_x=5.0, Ro_z=2.5
Ro_x=7.5, Ro_z=2.5
Ro_x=11.0, Ro_z=2.5
Ro_x=15.0, Ro_z=2.5
$\overline{u\theta}$
0.2
0.1
0.0
-0.1
-1.0
-0.5
0.0
0.5
1.0
y/δ

(a)

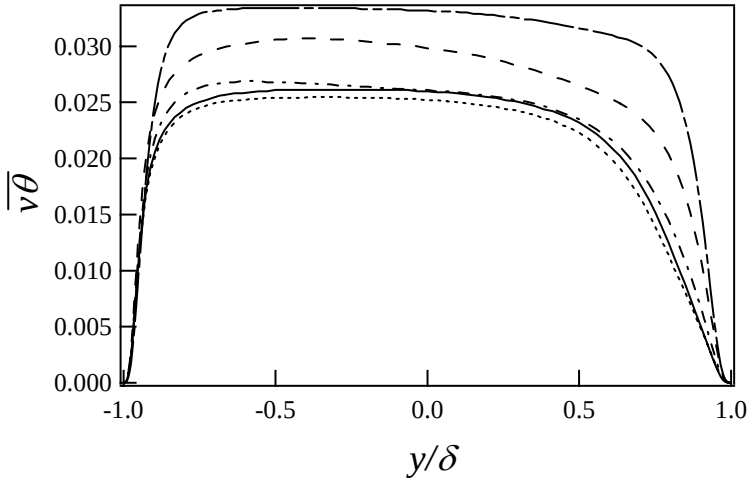
$\overline{v\theta}$
0.030
0.025
0.020
0.015
0.010
0.005
0.000
-1.0
-0.5
0.0
0.5
1.0
y/δ

(b)

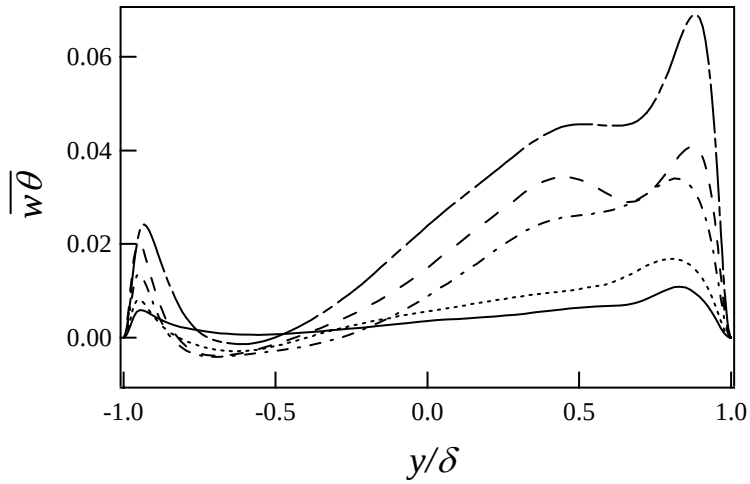
$\overline{w\theta}$
0.06
0.04
0.02
0.00
-1.0
-0.5
0.0
0.5
1.0
y/δ

(c)

Fig. 5

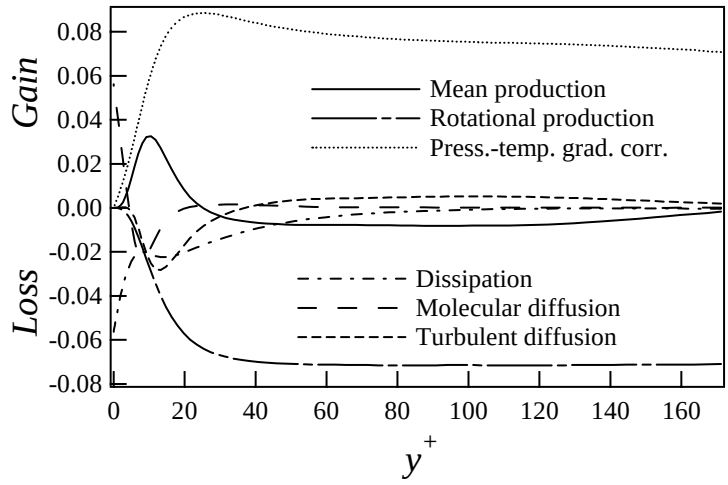
Gain
Loss
0.08
0.06
0.04
0.02
0.00
-0.02
-0.04
-0.06
-0.08
0
20
40
60
80
100
120
140
160
y^+
Mean production
Rotational production
Press.-temp. grad. corr.
Dissipation
Molecular diffusion
Turbulent diffusion

(a)

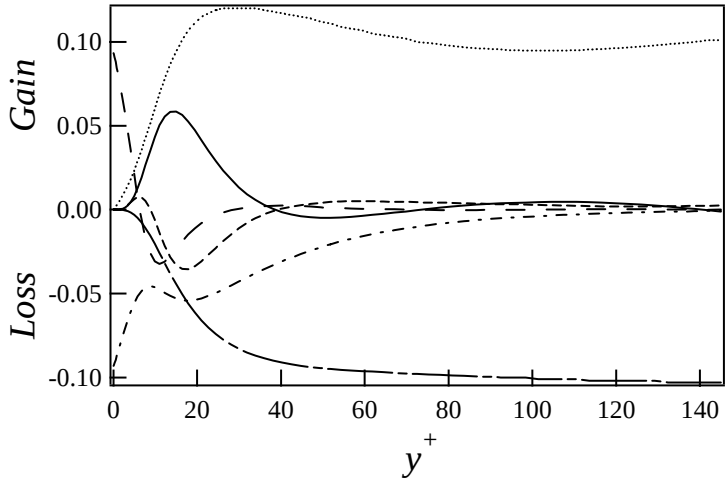
Gain
Loss
0.10
0.05
0.00
-0.05
-0.10
0
20
40
60
80
100
120
140
y^+

(b)

Fig. 6

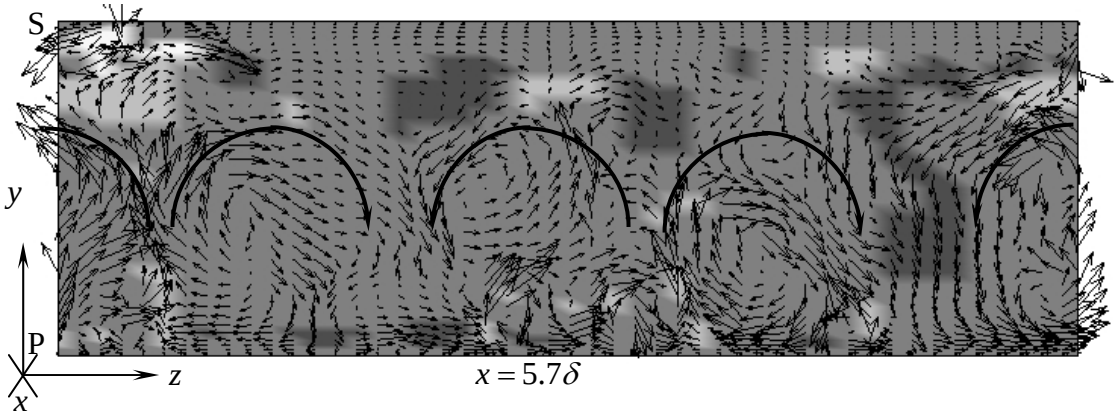
S
y
P
z
x
$x = 5.7\delta$

(a)

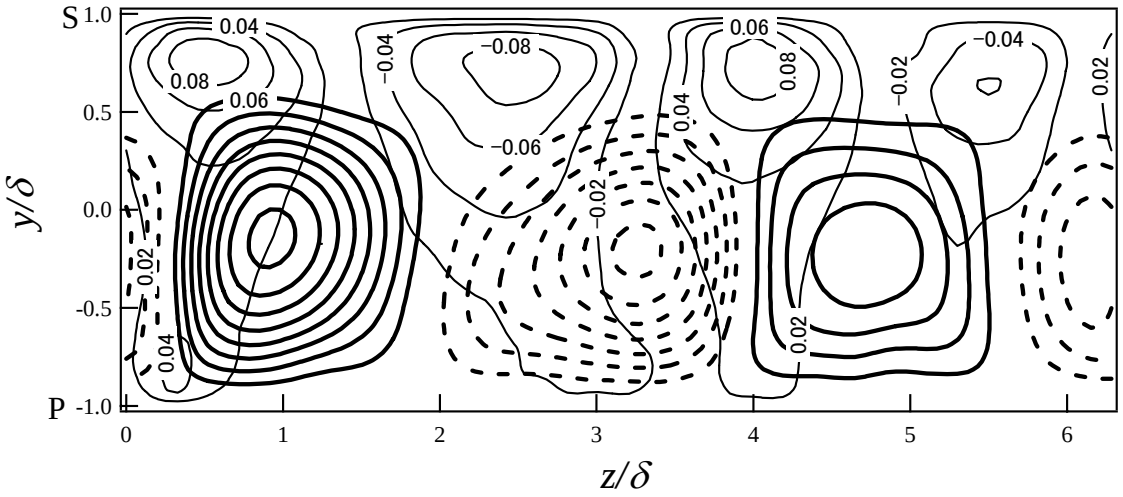
S
P
1.0
0.5
0.0
-0.5
-1.0
0
1
2
3
4
5
6
y/δ
z/δ
0.04
0.08
0.06
−0.04
−0.08
−0.06
−0.02
0.02

(b)

Fig. 7

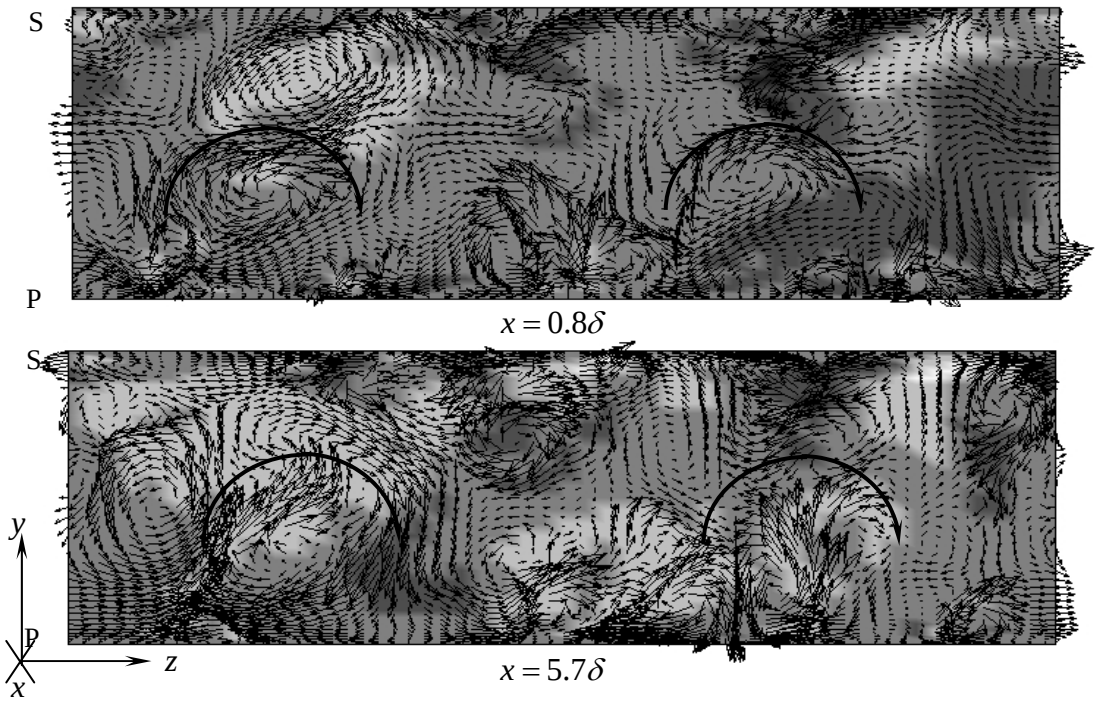
S
P
$x = 0.8\delta$
S
P
y
z
x
$x = 5.7\delta$

(a)

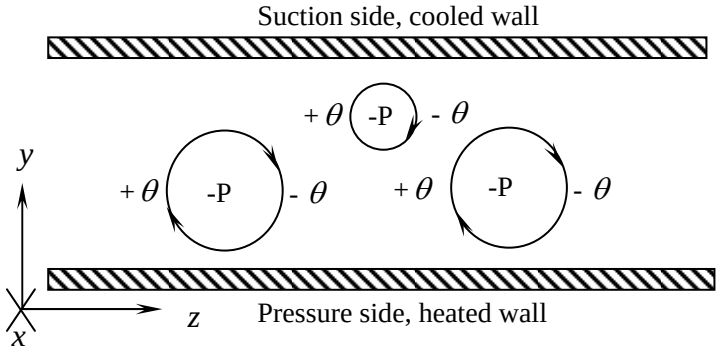
Suction side, cooled wall
+ θ
-P
- θ
+ θ
-P
- θ
+ θ
-P
- θ
y
z
x
Pressure side, heated wall

(b)

Fig. 8

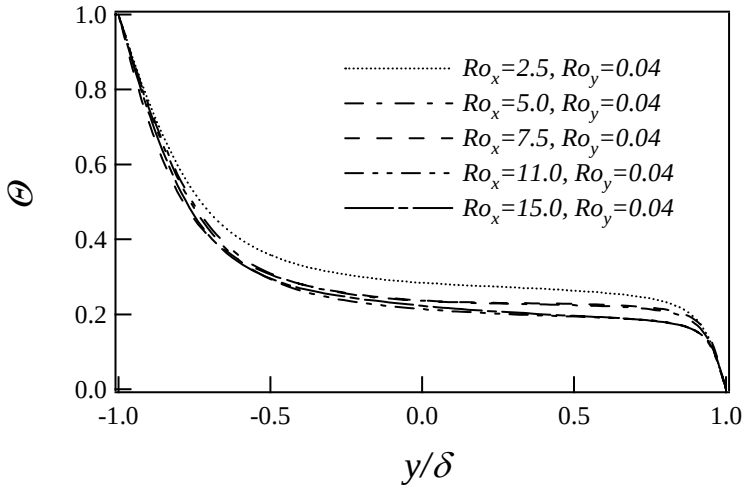
1.0
0.8
0.6
0.4
0.2
0.0
-1.0
-0.5
0.0
0.5
1.0
Θ
y/δ
Ro_x=2.5, Ro_y=0.04
Ro_x=5.0, Ro_y=0.04
Ro_x=7.5, Ro_y=0.04
Ro_x=11.0, Ro_y=0.04
Ro_x=15.0, Ro_y=0.04

(a)

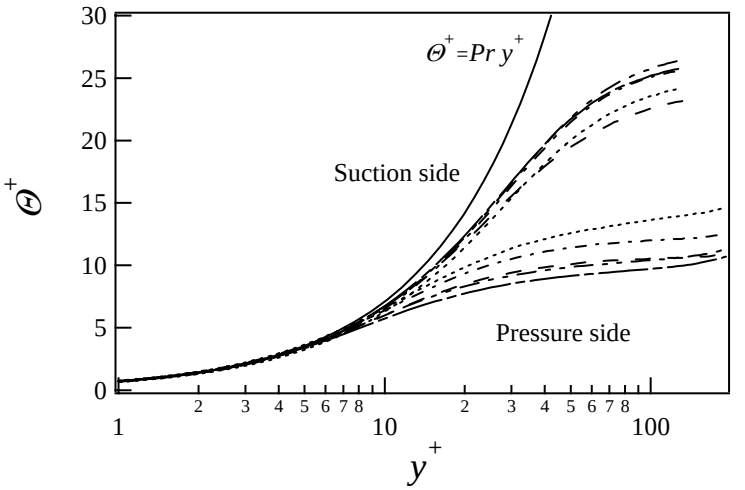
30
25
20
15
10
5
0
1
10
100
2 3 4 5 6 7 8
Θ+
y+
Θ+=Pr y+
Suction side
Pressure side

(b)

Fig. 9

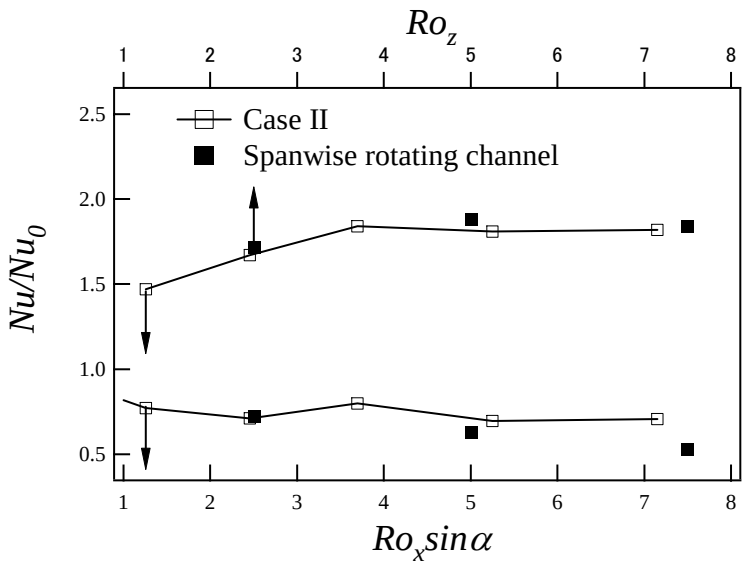
Ro_z
1
2
3
4
5
6
7
8
2.5
2.0
1.5
1.0
0.5
Case II
Spanwise rotating channel
Nu/Nu_0
$Ro_x sin\alpha$

Fig. 10

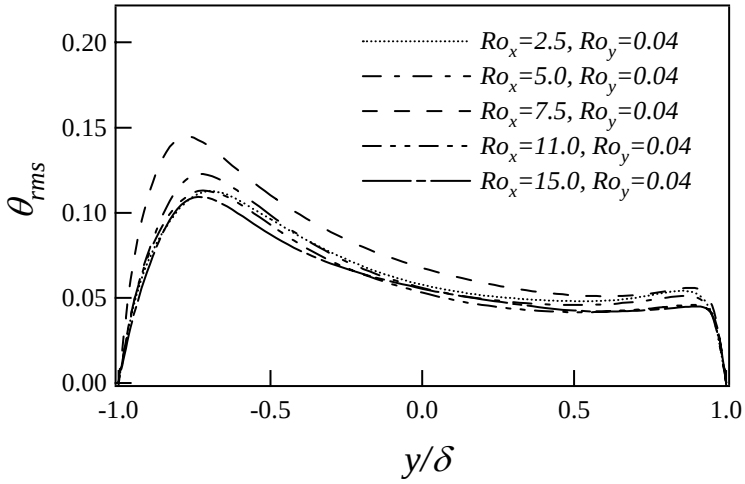
Ro_x=2.5, Ro_y=0.04
Ro_x=5.0, Ro_y=0.04
Ro_x=7.5, Ro_y=0.04
Ro_x=11.0, Ro_y=0.04
Ro_x=15.0, Ro_y=0.04
θ_{rms}
0.20
0.15
0.10
0.05
0.00
-1.0
-0.5
0.0
0.5
1.0
y/δ

(a)

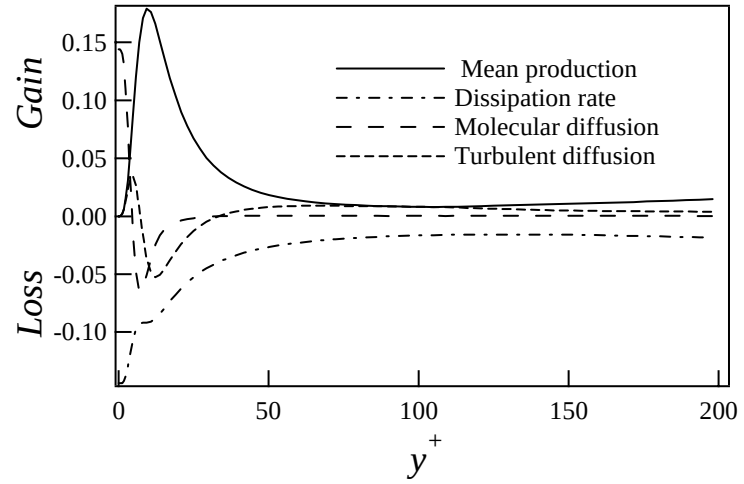
Mean production
Dissipation rate
Molecular diffusion
Turbulent diffusion
Gain
Loss
0.15
0.10
0.05
0.00
-0.05
-0.10
0
50
100
150
200
y^+

(b)

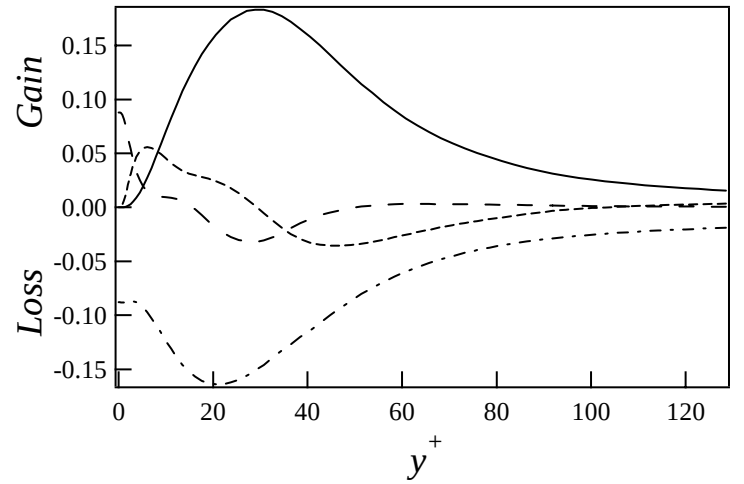
Gain
Loss
0.15
0.10
0.05
0.00
-0.05
-0.10
-0.15
0
20
40
60
80
100
120
y^+

(c)

Fig. 11

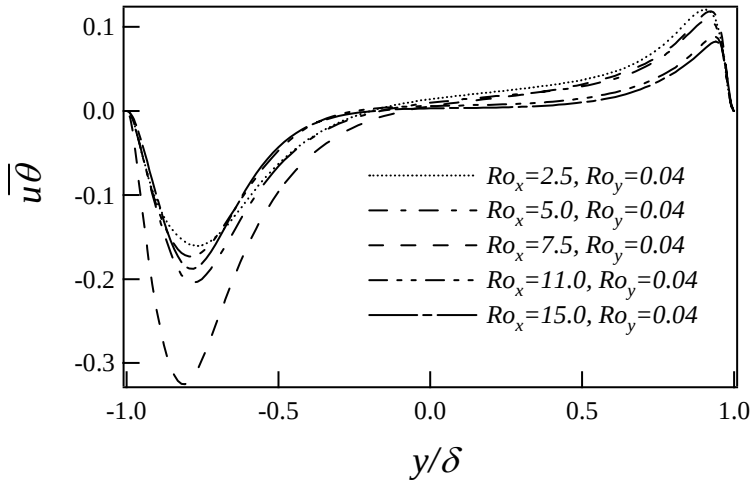
0.1
0.0
-0.1
-0.2
-0.3
$\overline{u\theta}$
Ro_x=2.5, Ro_y=0.04
Ro_x=5.0, Ro_y=0.04
Ro_x=7.5, Ro_y=0.04
Ro_x=11.0, Ro_y=0.04
Ro_x=15.0, Ro_y=0.04
-1.0
-0.5
0.0
0.5
1.0
y/δ

(a)

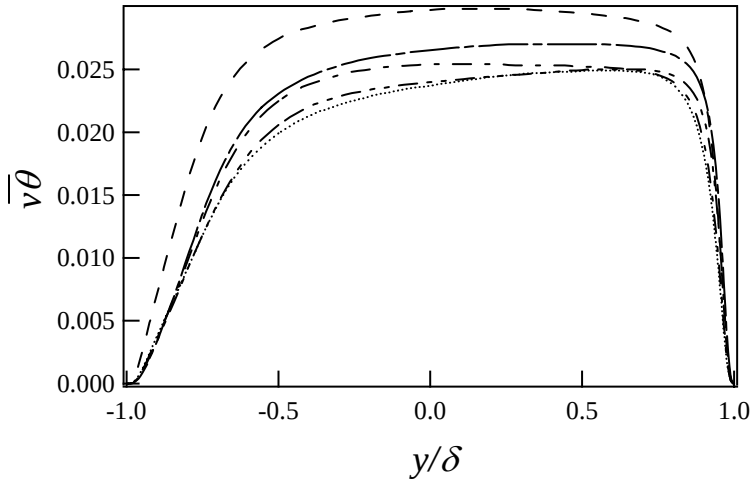
0.025
0.020
0.015
0.010
0.005
0.000
$\overline{v\theta}$
-1.0
-0.5
0.0
0.5
1.0
y/δ

(b)

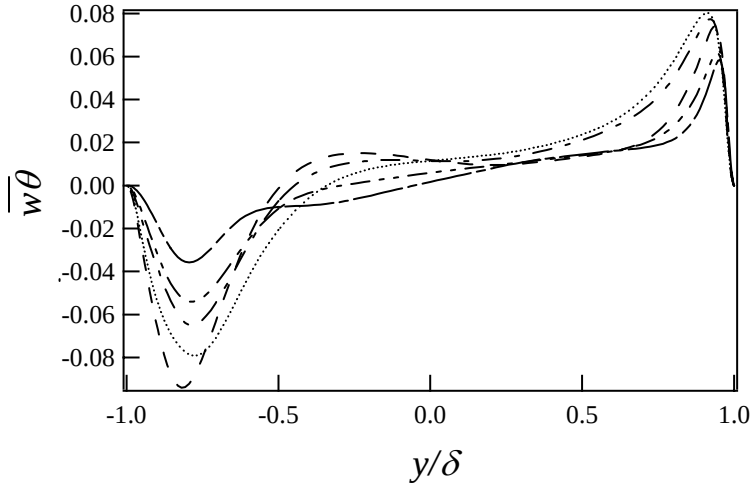
0.08
0.06
0.04
0.02
0.00
-0.02
-0.04
-0.06
-0.08
$\overline{w\theta}$
-1.0
-0.5
0.0
0.5
1.0
y/δ

(c)

Fig. 12

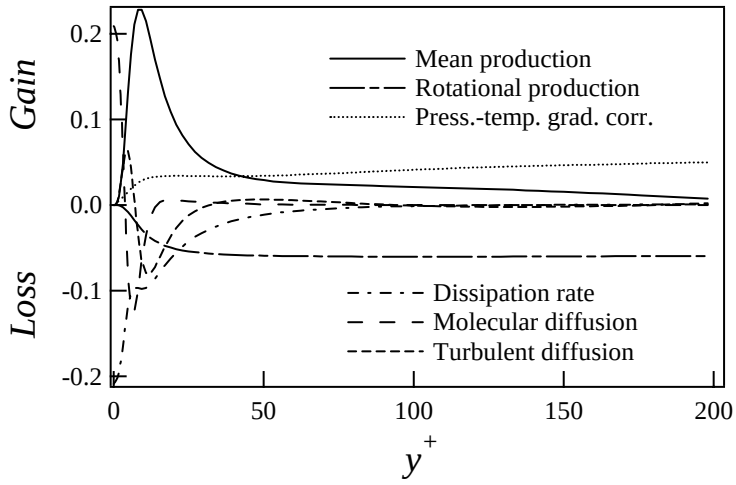
Gain
Loss
0.2
0.1
0.0
-0.1
-0.2
0
50
100
150
200
y^+
Mean production
Rotational production
Press.-temp. grad. corr.
Dissipation rate
Molecular diffusion
Turbulent diffusion

(a)

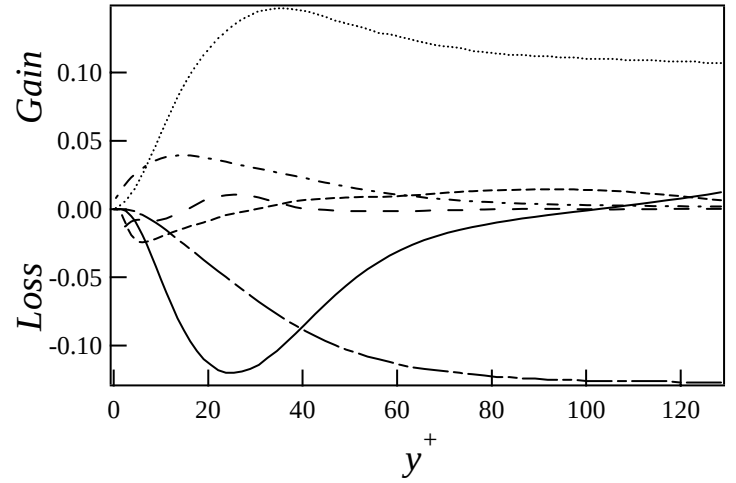
Gain
Loss
0.10
0.05
0.00
-0.05
-0.10
0
20
40
60
80
100
120
y^+

(b)

Fig. 13

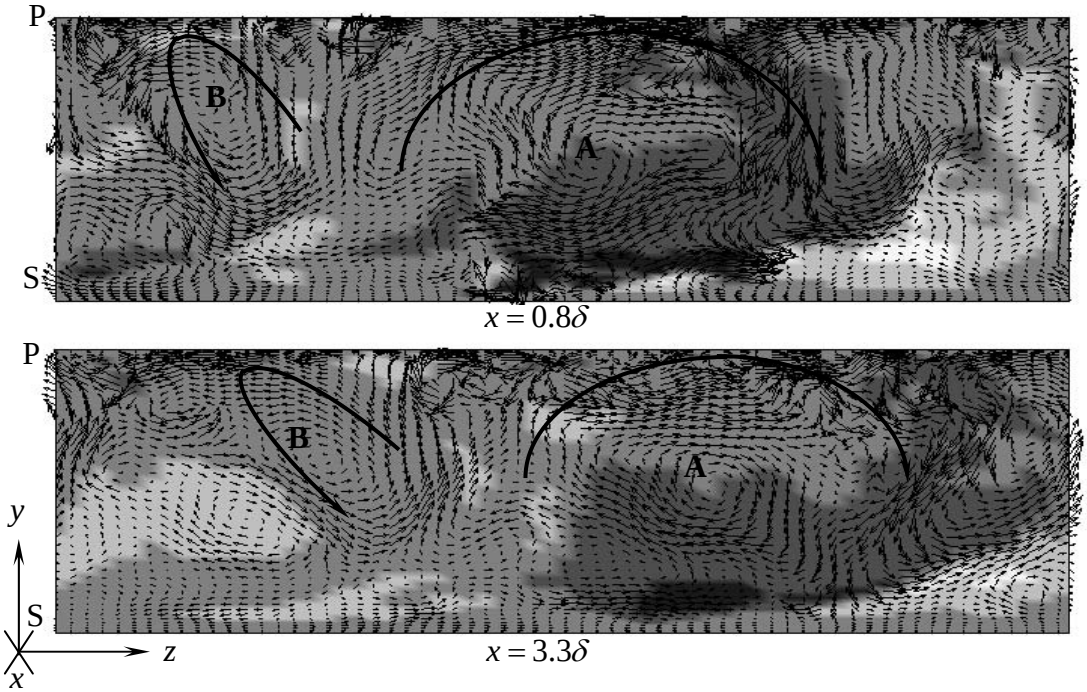

Fig. 14

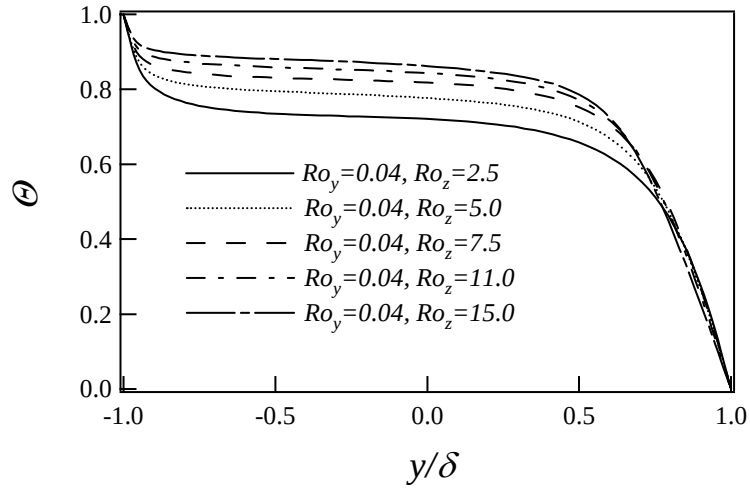
1.0
0.8
0.6
0.4
0.2
0.0
Θ
Ro_y=0.04, Ro_z=2.5
Ro_y=0.04, Ro_z=5.0
Ro_y=0.04, Ro_z=7.5
Ro_y=0.04, Ro_z=11.0
Ro_y=0.04, Ro_z=15.0
-1.0
-0.5
0.0
0.5
1.0
y/δ

(a)

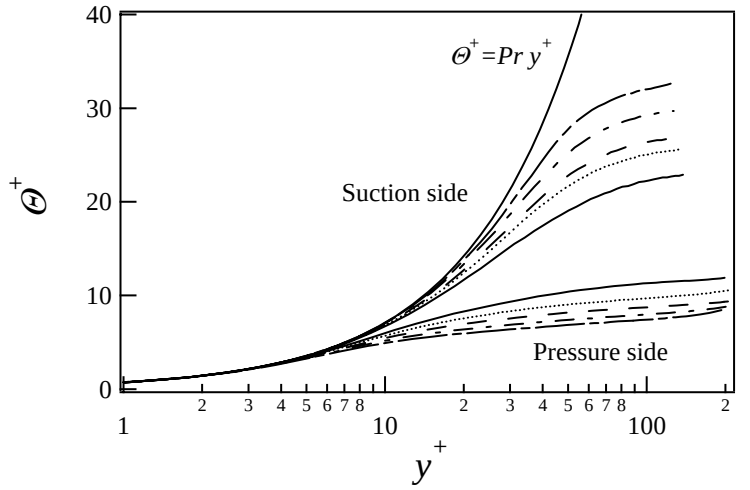
40
30
20
10
0
Θ+
Θ+=Pr y+
Suction side
Pressure side
1
10
100
y+

(b)

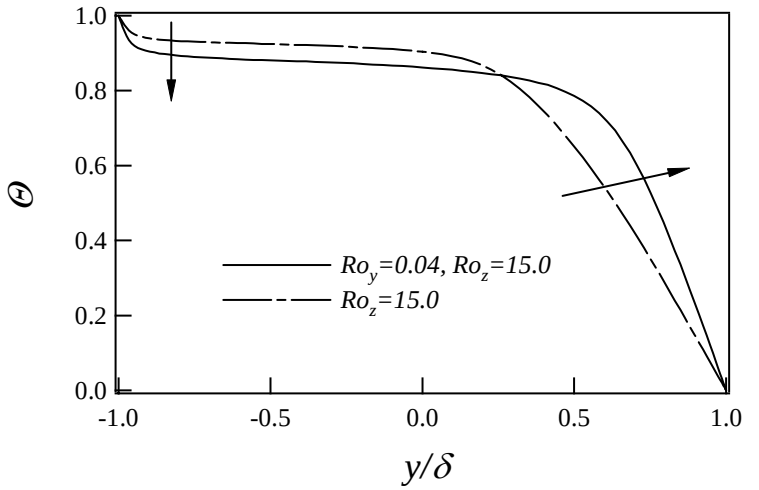
1.0
0.8
0.6
0.4
0.2
0.0
Θ
Ro_y=0.04, Ro_z=15.0
Ro_z=15.0
-1.0
-0.5
0.0
0.5
1.0
y/δ

(c)

Fig. 15

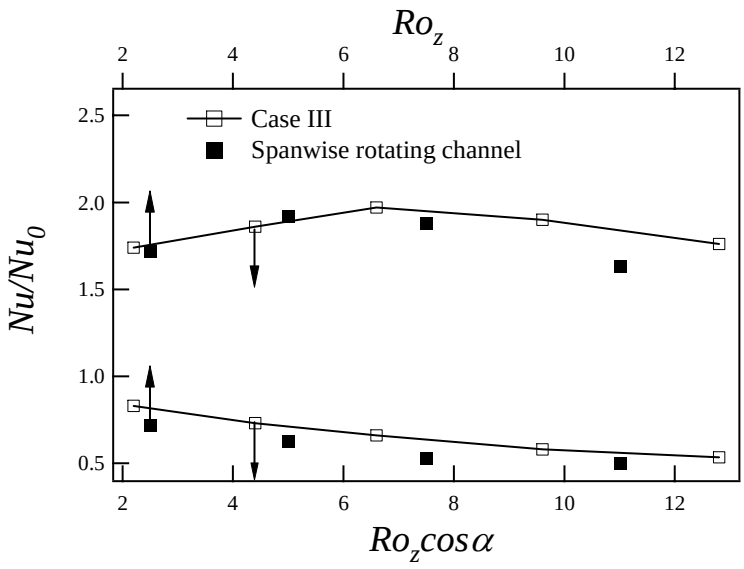
Ro_z
2
4
6
8
10
12
2.5
2.0
1.5
1.0
0.5
Case III
Spanwise rotating channel
Nu/Nu_0
$Ro_z cos\alpha$

Fig. 16

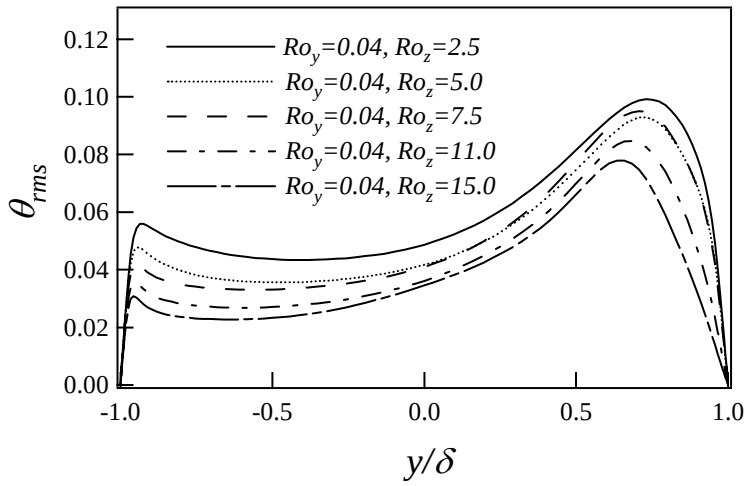
Ro_y=0.04, Ro_z=2.5
Ro_y=0.04, Ro_z=5.0
Ro_y=0.04, Ro_z=7.5
Ro_y=0.04, Ro_z=11.0
Ro_y=0.04, Ro_z=15.0
θ_{rms}
0.12
0.10
0.08
0.06
0.04
0.02
0.00
-1.0
-0.5
0.0
0.5
1.0
y/δ

(a)

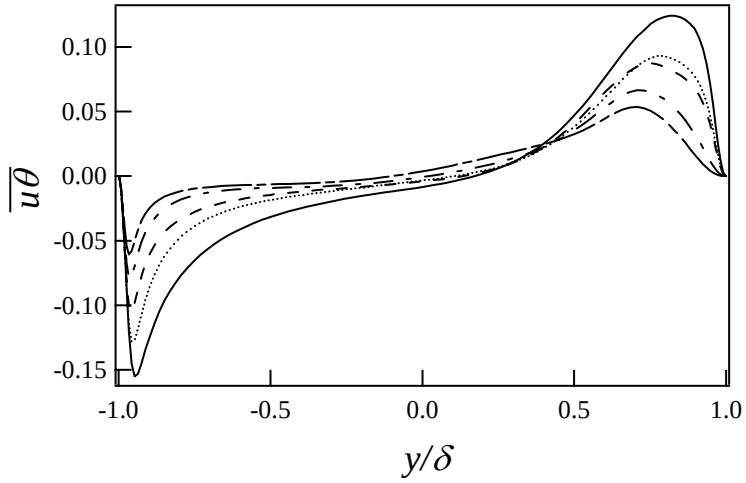
$\overline{u\theta}$
0.10
0.05
0.00
-0.05
-0.10
-0.15
-1.0
-0.5
0.0
0.5
1.0
y/δ

(b)

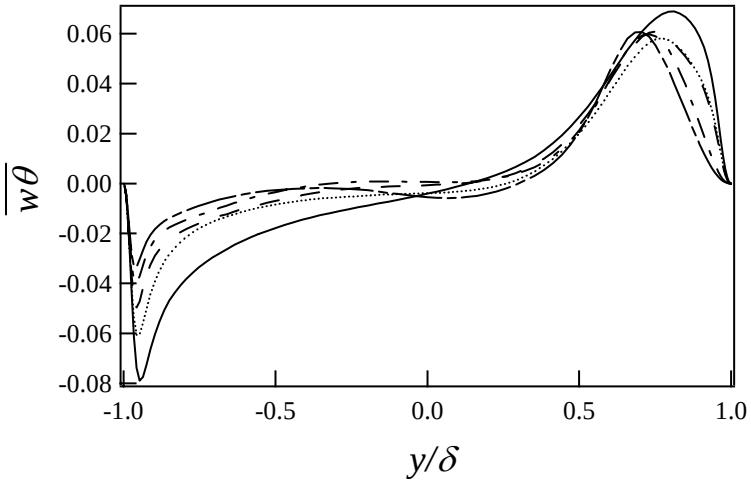
$\overline{w\theta}$
0.06
0.04
0.02
0.00
-0.02
-0.04
-0.06
-0.08
-1.0
-0.5
0.0
0.5
1.0
y/δ

(c)

Fig. 17

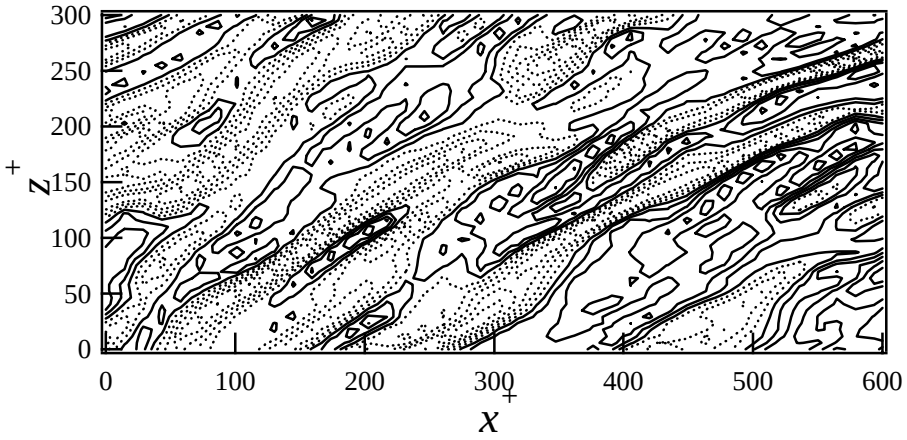
300
250
200
150
100
50
0
z^+
0
100
200
300
400
500
600
x^+

(a)

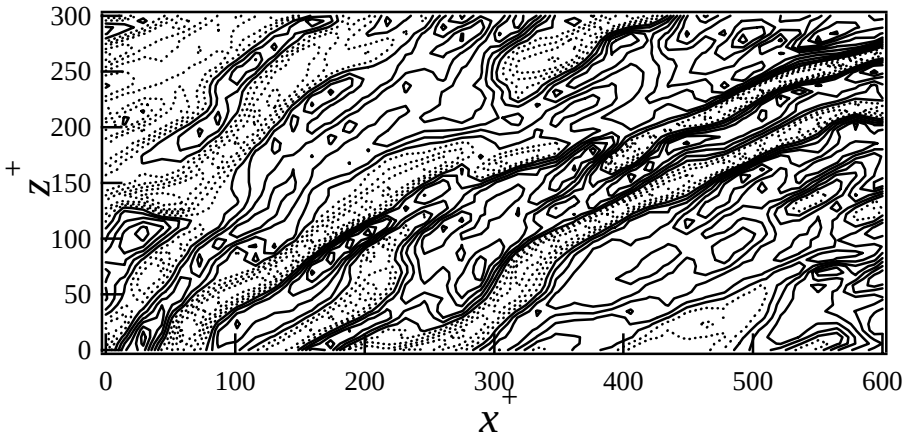
300
250
200
150
100
50
0
z^+
0
100
200
300
400
500
600
x^+

(b)

Fig. 18